

Bipolar seesaw in the northeastern tropical Atlantic during Heinrich stadials

Michelle Zarriess,¹ Heather Johnstone,^{2,3} Matthias Prange,^{2,3} Silke Steph,³
Jeroen Groeneveld,^{1,2,3} Stefan Mulitza,^{2,3} and Andreas Mackensen¹

Received 9 November 2010; revised 14 December 2010; accepted 28 December 2010; published 23 February 2011.

[1] Two SST records based on Mg/Ca of *G. ruber* (pink) from the continental slope off West Africa at 15°N and 12°N shed new light on the thermal bipolar seesaw pattern in the northeastern tropical Atlantic during periods of reduced Atlantic Meridional Overturning Circulation (AMOC) associated with Heinrich stadials H1 to H6. The two records indicate that the latitudinal position of the bipolar seesaw's zero-anomaly line, between cooling in the North and warming in the South, gradually shifted southward from H6 to H1. A conceptual model is presented that aims to provide a physically consistent mechanism for the southward migration of the seesaw's fulcrum. The conceptual model suggests latitudinal movements of the Intertropical Convergence Zone, driven by a combination of orbital-forced changes in the meridional temperature gradient within the realm of the Hadley cell and the expansion of the Northern Hemisphere cryosphere, as a major factor. **Citation:** Zarriess, M., H. Johnstone, M. Prange, S. Steph, J. Groeneveld, S. Mulitza, and A. Mackensen (2011), Bipolar seesaw in the northeastern tropical Atlantic during Heinrich stadials, *Geophys. Res. Lett.*, 38, L04706, doi:10.1029/2010GL046070.

1. Introduction

[2] The thermal bipolar seesaw - the cooling of the Northern Hemisphere associated with warming of the Southern Hemisphere - is a typical feature of millennial-scale climate variability during the last ice age [e.g., *Mix et al.*, 1986; *Crowley*, 1992; *Stocker*, 1998; *Rahmstorf*, 2002; *Stocker and Johnsen*, 2003]. It has been suggested that variations in the Atlantic Meridional Overturning Circulation (AMOC), and in the associated heat transport, qualify as the primary driver for such contrasting temperature evolution [e.g., *Crowley*, 1992; *Clark et al.*, 2002; *Rahmstorf*, 2002; *Stocker and Johnsen*, 2003; *Stouffer et al.*, 2006]. The seesaw pattern is clearly expressed in temperature records measured on ice cores from Greenland and Antarctica [e.g., *NGRIP Members*, 2004; *EPICA Community Members*, 2006], as well as in sea surface temperature (SST) records from the extratropical northern and southern Atlantic [*de Abreu et al.*, 2003; *Barker et al.*, 2009].

[3] In the tropical regions, however, not much is known about the spatial structure of the thermal bipolar seesaw.

Modeling studies suggest that the “zero-anomaly line” between AMOC-induced cooling in the north and warming in the south is located between 10°N and 15°N in the northeastern tropical Atlantic [*Stouffer et al.*, 2006]. Here, we use Mg/Ca based SST records measured on two sediment cores from this region (gravity core GeoB9508-5 from 15°29.9'N, 17°56.88'W, 2,384 m water depth and GeoB9526-5 from 12°26.1'N, 18°03.4'W, 3,231 m water depth) to test the model findings. Today, these core locations are strongly influenced by seasonal changes in the tropical wind field. During boreal summer, the northeast trade winds are weak and the Intertropical Convergence Zone (ITCZ) is at a northern position. The tropical rainbelt delivers precipitation into the Sahel region, initiating increased fluvial discharge into the Atlantic Ocean. During boreal winter, the northeast trades strengthen and the ITCZ and the tropical rainbelt shift towards the equator, accompanied by sea surface cooling and the southward expansion of dry conditions on the West African continent. In the present paper, we suggest that orbital- and cryosphere-driven changes in the position of the ITCZ determine the location of the seesaw's zero-anomaly line in the tropical Atlantic during Heinrich stadials.

2. Material and Methods

[4] The two gravity cores were recovered from the continental slope off West Africa during RV Meteor cruise M65/1 in 2005. For this study, core GeoB9508-5 was sampled between 80 and 950 cm (5 cm spacing), and GeoB9526-5 was sampled between 80 and 1000 cm (5 cm spacing). All samples were wet-sieved through a 63 μm mesh, oven-dried at 50°C and subsequently dry-sieved through 125 μm , 315 μm and 400 μm meshes.

[5] For Mg/Ca based temperature reconstructions, 20 to 25 visually uncontaminated tests of the planktic foraminiferal species *G. ruber* (pink) were selected from the narrow 315–400 μm size fraction to minimize size-related intra-specific elemental variations [*Elderfield et al.*, 2002]. The tests were cleaned in successive steps following the cleaning protocol of *Barker et al.* [2003] and analyzed on a Perkin-Elmer Optima 3300R ICP-OES at the Department of Geosciences, University of Bremen. Based on standards and replicate analyses, the mean reproducibility was ± 0.012 mmol/mol. Mg/Ca ratios were converted to SST using the *Regenberg et al.* [2009] species-specific calibration for *G. ruber* (pink) in the tropical Atlantic based on annual SST (see auxiliary material).¹

¹Alfred Wegener Institute for Polar and Marine Research, Bremerhaven, Germany.

²Center for Marine Environmental Sciences, University of Bremen, Bremen, Germany.

³Geosciences Department, University of Bremen, Bremen, Germany.

[6] In order to establish a continental aridity record for southern West Africa [Mulitza *et al.*, 2008], we determined Fe/K ratios in the bulk sediment of core GeoB9526-5 (see auxiliary material). Fe/K ratios in the study area are suggested to vary with changes in humidity and monsoonal precipitation [Mulitza *et al.*, 2008], since Fe/K values of atmospheric dust samples increase from the Sahel–Saharan region to the tropics [Stuut *et al.*, 2005]. Increasing amounts of dust derived from deeply weathered terrains [Moreno *et al.*, 2006] cause an increase of Fe/K ratios towards the tropics, because of its relatively high concentration of iron in comparison to more mobile potassium [Mulitza *et al.*, 2008]. In addition, Fe/K values of fluvial sediments are higher than those of eolian sediments [Stuut *et al.*, 2005; Mulitza *et al.*, 2008]. Highest water discharge, and therefore highest sedimentary load of the rivers, occurs during rainy seasons [e.g., Lesack *et al.*, 1984]. The elemental intensities of Fe and K were measured with an AVAATECH X-ray fluorescence (XRF) scanner at scanning steps of 1 cm, using a generator setting of 10 kV and 0.3 mA and a detection time of 30 seconds. Fe/K ratios for the upper 365 cm of core GeoB9526-5 are already given by Zarriess and Mackensen [2010].

[7] The age model for core GeoB9508-5 is based on 12 accelerator mass spectrometry (AMS) radiocarbon dates on planktic foraminifera and correlation of the benthic $\delta^{18}\text{O}$ record with core MD95-2042 [Shackleton *et al.*, 2004; Mulitza *et al.*, 2008]. For core GeoB9526-5, we established an age model based on 7 AMS radiocarbon dates (Figure 1) [Zarriess and Mackensen, 2010], which were determined on mixed planktic foraminifera ($>125\ \mu\text{m}$) at the Leibniz-Laboratory for Radiometric Dating and Stable Isotope Research, Kiel, Germany [Nadeau *et al.*, 1997] (see auxiliary material). The conventional radiocarbon ages were corrected for a reservoir effect of 400 years and converted to calendar ages using the “Fairbanks0107” calibration curve [Fairbanks *et al.*, 2005].

[8] To extend the age model for core GeoB9526-5 beyond the range of radiocarbon dating, we determined the stable oxygen isotopic composition of the epibenthic foraminifer *Cibicidoides wuellerstorfi* (see auxiliary material). Two to five specimens ($>125\ \mu\text{m}$) were measured on a Finnigan MAT 251 isotope ratio mass spectrometer coupled to an automatic carbonate preparation device (Kiel II). All oxygen isotope values are given in δ notation versus Vienna Pee Dee belemnite standard (VPDB). The external reproducibility is better than $\pm 0.08\text{‰}$. The GeoB9526-5 benthic $\delta^{18}\text{O}$ record was correlated with the benthic $\delta^{18}\text{O}$ records of GeoB9508-5 [Mulitza *et al.*, 2008] and MD95-2042 [Shackleton *et al.*, 2004] by means of AnalySeries 1.1.1 (D. Paillard *et al.*, Analyseries. Computer program for graphical correlation on a Macintosh, edited, 1992), resulting in seven additional age tie points (Figure 1). Sedimentation rates in core GeoB9526-5 vary between $7.7\ \text{cm kyr}^{-1}$ and $29\ \text{cm kyr}^{-1}$ (see auxiliary material).

3. Results

[9] The Mg/Ca based SST records from both core locations, GeoB9508-5 at 15°N and GeoB9526-5 at 12°N , reveal pronounced millennial-scale variability mainly associated with AMOC slowdown during North Atlantic Heinrich stadials (H6–H1) (Figures 1c and 1e). During H6, SST at the southern core GeoB9526-5 (12°N) increased by $\sim 1^\circ\text{C}$ (no data are available for core GeoB9508-5 at 15°N).

During the cold stadial recorded in Greenland ice cores between Dansgaard-Oeschger warm events 14 and 15 (54–56 kyr BP; H5/6 in Figure 1), warming occurred at 12°N as well as at 15°N . During H5, H4 and H3, the paleotemperature records from 12°N and 15°N display opposing SST anomalies; warming at the southern core location (GeoB9526-5) was accompanied by cooling at the northern core location (GeoB9508-5). Heinrich stadials H2 and H1, however, were characterized by a moderate cooling at both core locations (12°N and 15°N) (Figures 1c and 1e).

[10] Fe/K ratios at site GeoB9526-5 (12°N) also exhibit millennial-scale variations coinciding with Heinrich stadials (Figure 1f). Times of AMOC weakening (H6–H1) are generally characterized by low Fe/K ratios, indicative of dry conditions over southern West Africa [cf. Mulitza *et al.*, 2008]. This distinct short-term variability overlies a long-term increase in Fe/K ratios between Marine Isotope Stage (MIS) 4 and early MIS 3 (72–53 kyr BP) and a long-term decrease in Fe/K ratios between early MIS 3 and MIS 2 (53–20 kyr BP; Figure 1f).

4. Discussion

4.1. Physics of the Tropical Seesaw

[11] Weakening of the AMOC increases the heat content of the tropical Atlantic (20°S – 20°N) due to reduced import of relatively cold-water from the south and reduced warm-water export to the north [Chiang *et al.*, 2008]. This pattern is replicated by climate models, which show a widespread warming of the tropical Atlantic down to $>1000\ \text{m}$ depth in response to AMOC slowdown except for a thin surface layer in the tropical North Atlantic which exhibits cold temperature anomalies [e.g., Stouffer *et al.*, 2006; Stocker *et al.*, 2007; Zhang, 2007]. Analysis of the surface heat budget in freshwater hosing experiments reveal that the surface cooling in the tropical North Atlantic is predominantly caused by enhanced evaporative latent heat fluxes [Zhang, 2007; Chiang *et al.*, 2008]. These anomalous evaporative fluxes result from strengthened northeasterly trade winds, while the southeasterly trades weaken due to an overall northerly wind anomaly over the tropical Atlantic [Timmermann *et al.*, 2007; Chiang *et al.*, 2008].

[12] Our own analysis of a freshwater hosing experiment with the fully coupled Community Climate System Model (version CCSM2/T31x3a [Prange, 2008]; a detailed description of the model experiment is given by Mulitza *et al.* [2008]) reveals that annual-mean surface latent heat flux anomalies exceed $12\ \text{W/m}^2$ off the coast of West Africa at the locations of GeoB9508-5 and GeoB9526-5 in response to a slowdown of the AMOC from $\sim 12\ \text{Sv}$ to $\sim 2\ \text{Sv}$ (not shown). By contrast, anomalies of sensible heat fluxes are well below $2.5\ \text{W/m}^2$ in that region, while the anomaly of net radiative (shortwave plus longwave) flux into the ocean is slightly positive ($<3\ \text{W/m}^2$), mainly due to reduced cloudiness. Likewise, anomalies of vertical advective heat fluxes due to changes in large-scale Ekman divergence are negligible in the region of core sites GeoB9508-5 and GeoB9526-5 (note, however, that coastal upwelling cannot be resolved in a coarse-resolution global model like CCSM2/T31x3a).

[13] Obviously, the evaporative cooling in the tropical North Atlantic through strengthened northeasterly trade winds is closely linked to the position of the Atlantic ITCZ. A more southward position of the ITCZ increases the area of

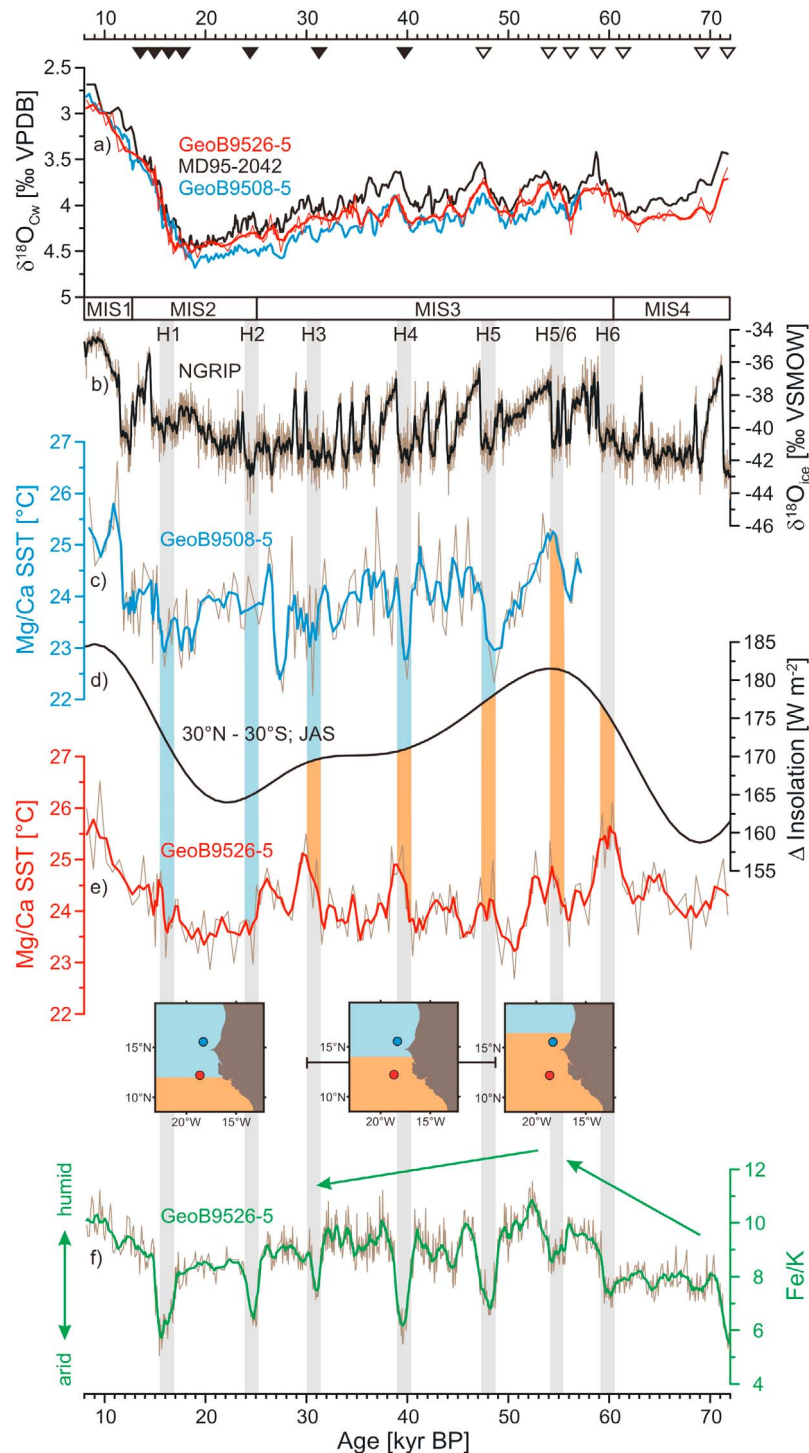


Figure 1. (a) Age model of sediment core GeoB9526-5 based on Accelerator Mass Spectrometer radiocarbon dates (filled triangles) and age tie points (open triangles) derived by correlation of benthic $\delta^{18}\text{O}$ record of cores GeoB9526-5 (red), GeoB9508-5 (black) [Mulitza *et al.*, 2008] and MD95-2042 (blue) [Shackleton *et al.*, 2004]. Comparison of (b) $\delta^{18}\text{O}$ of Greenland ice core (North Greenland Ice Core Project), and (d) summer (June 21–September 21) insolation difference between 30°N and 30°S with down core variations of (c, e) Mg/Ca-based sea surface temperature from sediment cores GeoB9508-5 and GeoB9526-5 and (f) Fe/K values from GeoB9526-5. Heinrich stadials (H1 – H6) are indicated by grey bars based on Greenland ice core $\delta^{18}\text{O}$. Orange (light blue) bars mirror SST warming (cooling) associated with Heinrich stadials. The insets schematically illustrate the inferred position of the SST zero-anomaly line with respect to the core locations (red dot: GeoB9526-5; blue dot: GeoB9508-5).

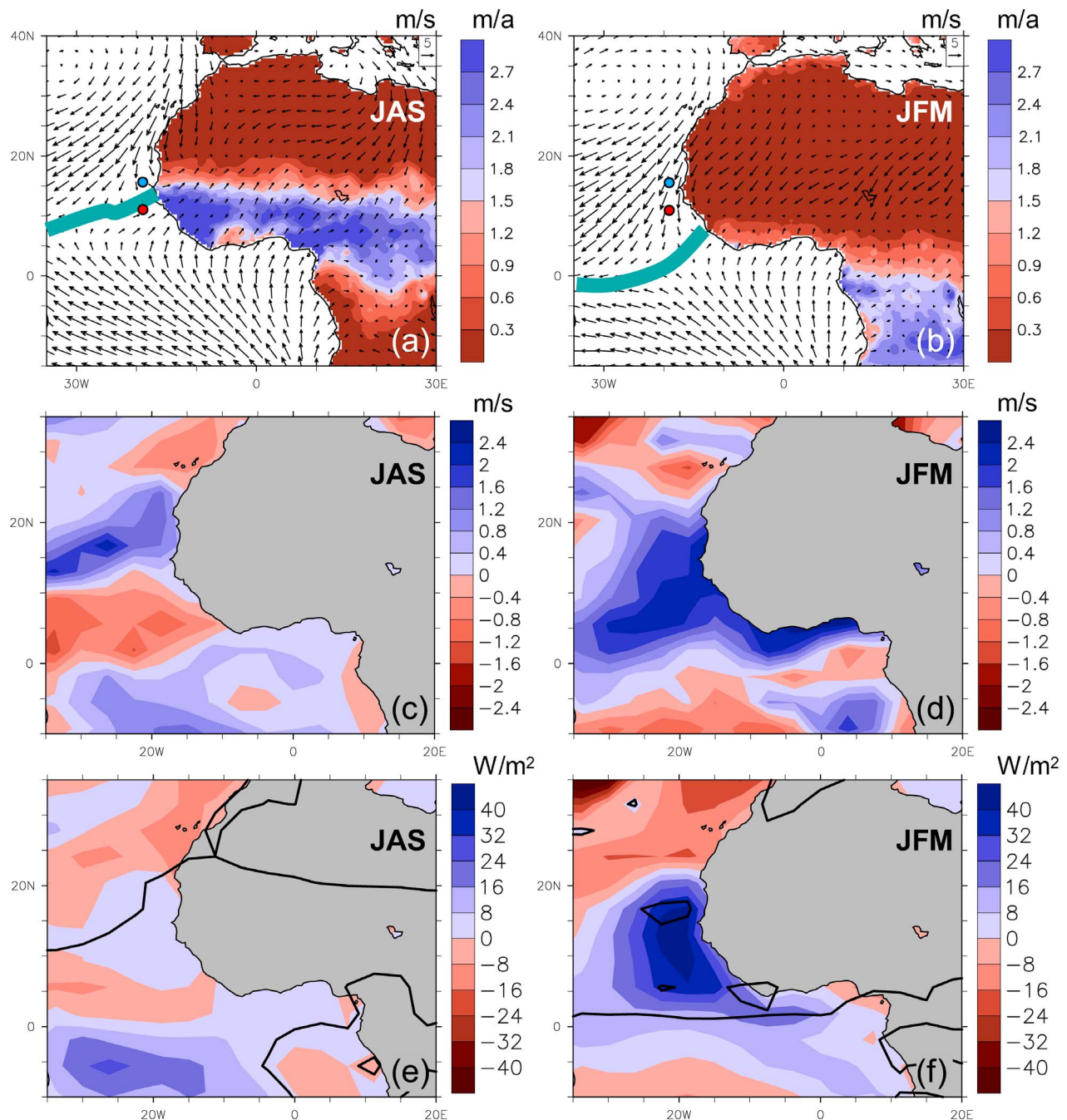


Figure 2. Climatological mean continental precipitation and near-surface winds for (a) July–September and (b) January–March as calculated from observational (University of Delaware, <http://climate.geog.udel.edu/~climate/>) and reanalysis data [Kalnay *et al.*, 1996]. The position of the Atlantic ITCZ (cyan line; represented by the zero-isoline of meridional wind velocity) and the core locations (red dot: GeoB9526-5; blue dot: GeoB9508-5) are highlighted. Climatic response to a substantial AMOC weakening as simulated in our freshwater-hosing experiment: (c) summer (July–September) and (d) winter (January–March) mean wind speed anomalies, (e) summer and (f) winter mean latent heat flux anomalies along with surface temperature zero-anomaly lines. All anomalies were calculated as differences of long-term (100 years) averaged fields between the water-hosing experiment and the control run.

northeasterly trade wind dominance over the tropical Atlantic, giving rise to a larger area of evaporative cooling upon AMOC slowdown. By contrast, a more northern position of the Atlantic ITCZ enhances the influence of the southeasterly trades that are weakened rather than strengthened in response to AMOC slowing. This is best illustrated

by comparing the tropical wind-field response of summer with that of winter, i.e., when the Atlantic ITCZ is located at an extremely northern (boreal summer) and southern (boreal winter) position (Figures 2a and 2b). Figure 2 shows the results from our CCSM2/T31x3a water-hosing experiment.

In summer, when the Atlantic ITCZ is located at its northernmost position (Figure 2a), the northerly surface wind anomaly that is induced by AMOC slowdown decelerates the climatological southeasterlies south of the latitude of Cape Verde. Consequently, surface wind speeds and hence latent heat fluxes are reduced in the North Atlantic south of $\sim 10^{\circ}\text{N}$ and the SST zero-anomaly line migrates northward (Figures 2c and 2e). In boreal winter, when the ITCZ reaches its southernmost position (Figure 2b), amplified northeast trades cause enhanced evaporative cooling in the eastern tropical Atlantic between 20°N and the equator (Figures 2d and 2f). As a result, the SST zero-anomaly line migrates towards the equator (Figure 2f).

4.2. A Conceptual Model for the Southward Migration of the Seesaw's Fulcrum

[14] Based on the results from the previous section, we suggest that the change in the position of the SST zero-anomaly line during Heinrich stadials through MIS4-MIS2 indicated by our Mg/Ca SST records was linked to the latitudinal position of the Atlantic ITCZ. While we surmise that in boreal winter, the ITCZ was always sufficiently far south, such that enhanced wind speeds of intensified northeast trades during Heinrich stadials resulted in evaporative heat loss at both core sites, we assume that it was the summer position of the ITCZ which was crucial for the pattern of the tropical SST seesaw.

[15] Around H5/6 (54–56 kyr BP; Figure 1), the (summer) ITCZ was located at a northern position, such that both core sites experienced SST warming during AMOC slowdown. A southward migration of the ITCZ during MIS3 gave rise to the anticorrelated SST changes found for H3–H5 (Figures 1c and 1e). During MIS2 the ITCZ was located at an extremely southern position such that both core sites experienced anomalous evaporative cooling due to intensified northeasterly trade winds during H2 and H1. In addition to evaporative heat fluxes enhanced coastal upwelling might have contributed to the H2 and H1 coolings at core site GeoB9526-5, when the global sea level was some 110 m lower than today [e.g., *Arz et al.*, 2007] and hence GeoB9526-5 was closer to the shoreline.

[16] The postulated long-term behaviour of the ITCZ on orbital timescales is corroborated by the Fe/K record (Figure 1f), which is indicative of continental rainfall. As precipitation over West Africa is linked to the position of the ITCZ, both the millennial-scale reduction in rainfall during Heinrich stadials [e.g., *Mulitza et al.*, 2008] and the orbital-scale long-term trends in the Fe/K records can be interpreted in terms of meridional movements of the ITCZ.

[17] We propose that the long-term movement of the ITCZ is primarily driven by two factors: (i) the meridional temperature gradient within the realm of the Hadley cell, and (ii) the expansion of Northern Hemisphere glaciation [*Flohn*, 1981; *Chiang and Bitz*, 2005]. As a driver for the first factor we suggest the summer insolation difference between 30°N and 30°S (Figure 1d), while the benthic oxygen isotope records (Figure 1a) are strongly related to glaciation in northern latitudes. Accordingly, the long-term trends of the Fe/K record (Figure 1f) are largely parallel to the benthic isotope records (Figure 1a) and the insolation curve (Figure 1d).

4.3. Caveat: Magnitude of AMOC Slowdown

[18] The conceptual model proposed in the previous section combines physically consistent processes with the paleorecord of West African rainfall that is associated with the position of the ITCZ. It does not exclude, however, that other mechanisms might have been responsible for the southward movement of the seesaw's zero-anomaly line. An obvious hypothesis might be that the magnitude of AMOC slowdown (associated with the magnitude of North Atlantic meltwater input and/or the stability properties of the AMOC) affected the position of the fulcrum. Some water-hosing model studies indeed suggest that the zero-anomaly line in the northeastern tropical Atlantic moves southward with increasing meltwater input [*Otto-Bliesner and Brady*, 2010]. Hence, different magnitudes of AMOC slowdown during Heinrich stadials cannot be ruled out as a potential cause for the different locations of the seesaw's fulcrum. However, the gradual southward movement of the fulcrum from MIS4 to MIS2 would imply a gradual increase in the magnitude of AMOC slowdown from H6 to H1, for which there is no paleoceanographic evidence. Applying appropriate boundary conditions for MIS4 and MIS3, climate modelling of different Heinrich events is urgently needed to disentangle the different effects of orbital forcing, cryosphere expansion and meltwater forcing upon the bipolar seesaw.

5. Conclusions

[19] Two records of SST (derived from Mg/Ca of *G. ruber* pink) from the West African margin at 15°N (GeoB9508-5) and 12°N (GeoB9526-5) during MIS 2–4 reveal variations in the latitudinal position of the bipolar seesaw's zero-anomaly, which separates Northern Hemisphere cooling from Southern Hemisphere warming. During H1 and H2, cooling at both core locations suggests a position of the zero-anomaly line south of 12°N . During H3 to H5, warming at the southern core location associated with cooling at the northern core location hints to a position of the zero-anomaly line between 12°N and 15°N . During subordinated cold stadial H5/6, warming at 12°N as well as 15°N indicates a position of the zero-anomaly line north of 15°N . We propose a conceptual model in which the observed modifications of the tropical seesaw SST pattern were driven by a long-term movement of the ITCZ summer position, which also affected rainfall over West Africa. We propose that the seesaw's zero-anomaly line is ultimately controlled by the interplay between orbital-driven changes in the tropical meridional temperature gradient and the expansion of Northern Hemisphere glaciation.

[20] **Acknowledgments.** We thank Günter Meyer, Lisa Schönborn, Cornelia Saukel and Susanne Wiebe for technical support. The climate model experiments have been performed on the IBM pSeries 690 Supercomputer of the Norddeutscher Verbund für Hoch- und Höchstleistungsrechnen (HLRN). This work was supported by the DFG Research Centre/Excellence Cluster "The Ocean in the Earth System."

References

- Arz, H. W., et al. (2007), Dominant Northern Hemisphere climate control over millennial-scale glacial sea-level variability, *Quat. Sci. Rev.*, 26(3–4), 312–321, doi:10.1016/j.quascirev.2006.07.016.
- Barker, S., M. Greaves, and H. Elderfield (2003), A study of cleaning procedures used for foraminiferal Mg/Ca paleothermometry, *Geochem. Geophys. Geosyst.*, 4(9), 8407, doi:10.1029/2003GC000559.

- Barker, S., et al. (2009), Interhemispheric Atlantic seesaw response during the last deglaciation, *Nature*, 457(7233), 1097–1102, doi:10.1038/nature07770.
- Chiang, J., and C. Bitz (2005), Influence of high latitude ice cover on the marine Intertropical Convergence Zone, *Clim. Dyn.*, 25(5), 477–496, doi:10.1007/s00382-005-0040-5.
- Chiang, J. C. H., W. Cheng, and C. M. Bitz (2008), Fast teleconnections to the tropical Atlantic sector from Atlantic thermohaline adjustment, *Geophys. Res. Lett.*, 35, L07704, doi:10.1029/2008GL033292.
- Clark, P. U., et al. (2002), The role of the thermohaline circulation in abrupt climate change, *Nature*, 415(6874), 863–869, doi:10.1038/415863a.
- Crowley, T. J. (1992), North Atlantic Deep Water cools the Southern Hemisphere, *Paleoceanography*, 7(4), 489–497, doi:10.1029/92PA01058.
- de Abreu, L., et al. (2003), Millennial-scale oceanic climate variability off the Western Iberian margin during the last two glacial periods, *Mar. Geol.*, 196(1–2), 1–20, doi:10.1016/S0025-3227(03)00046-X.
- Elderfield, H., M. Vautravers, and M. Cooper (2002), The relationship between shell size and Mg/Ca, Sr/Ca, $\delta^{18}\text{O}$, and $\delta^{13}\text{C}$ of species of planktonic foraminifera, *Geochem. Geophys. Geosyst.*, 3(8), 1052, doi:10.1029/2001GC000194.
- EPICA Community Members (2006), One-to-one coupling of glacial climate variability in Greenland and Antarctica, *Nature*, 444(7116), 195–198, doi:10.1038/nature05301.
- Fairbanks, R. G., et al. (2005), Radiocarbon calibration curve spanning 0 to 50,000 years BP based on paired $^{230}\text{Th}/^{234}\text{U}/^{238}\text{U}$ and ^{14}C dates on pristine corals, *Quat. Sci. Rev.*, 24(16–17), 1781–1796, doi:10.1016/j.quascirev.2005.04.007.
- Flohn, H. (1981), A hemispheric circulation asymmetry during late Tertiary, *Geol. Rundsch.*, 70, 725–736, doi:10.1007/BF01822146.
- Kalnay, E., et al. (1996), The NCEP/NCAR 40-year reanalysis project, *Bull. Am. Meteorol. Soc.*, 77(3), 437–471, doi:10.1175/1520-0477(1996)077<0437:TNYRP>2.0.CO;2.
- Lesack, L. F. W., et al. (1984), Transport of carbon, nitrogen, phosphorus, and major solutes in the Gambia River, West Africa, *Limnol. Oceanogr.*, 29(4), 816–830, doi:10.4319/lo.1984.29.4.0816.
- Mix, A. C., W. F. Ruddiman, and A. McIntyre (1986), Late Quaternary paleoceanography of the tropical Atlantic: 2. The seasonal cycle of sea surface temperatures, 0–20,000 years B.P., *Paleoceanography*, 1(3), 339–353, doi:10.1029/PA001i003p00339.
- Moreno, T., et al. (2006), Geochemical variations in aeolian mineral particles from the Sahara-Sahel Dust Corridor, *Chemosphere*, 65(2), 261–270, doi:10.1016/j.chemosphere.2006.02.052.
- Mulitza, S., M. Prange, J.-B. Stuut, M. Zabel, T. von Dobeneck, A. C. Itambi, J. Nizou, M. Schulz, and G. Wefer (2008), Sahel megadroughts triggered by glacial slowdowns of Atlantic meridional overturning, *Paleoceanography*, 23, PA4206, doi:10.1029/2008PA001637.
- Nadeau, M. J., et al. (1997), The Leibniz-Labor AMS facility at the Christian-Albrechts University, Kiel, Germany, *Nucl. Instrum. Methods Phys. Res., Sect. B*, 123(1–4), 22–30, doi:10.1016/S0168-583X(96)00730-6.
- NGRIP Members (2004), High-resolution record of Northern Hemisphere climate extending into the last interglacial period, *Nature*, 431(7005), 147–151, doi:10.1038/nature02805.
- Otto-Bliessner, B. L., and E. C. Brady (2010), The sensitivity of the climate response to the magnitude and location of freshwater forcing: Last Glacial Maximum experiments, *Quat. Sci. Rev.*, 29(1–2), 56–73, doi:10.1016/j.quascirev.2009.07.004.
- Prange, M. (2008), The low-resolution CCSM2 revisited: New adjustments and a present-day control run, *Ocean Sci.*, 4(2), 151–181, doi:10.5194/os-4-151-2008.
- Rahmstorf, S. (2002), Ocean circulation and climate during the past 120,000 years, *Nature*, 419(6903), 207–214, doi:10.1038/nature01090.
- Regenberg, M., et al. (2009), Calibrating Mg/Ca ratios of multiple planktonic foraminiferal species with $\delta^{18}\text{O}$ -calcification temperatures: Paleothermometry for the upper water column, *Earth Planet. Sci. Lett.*, 278(3–4), 324–336, doi:10.1016/j.epsl.2008.12.019.
- Shackleton, N. J., et al. (2004), Absolute calibration of the Greenland time scale: Implications for Antarctic time scales and for $\delta^{14}\text{C}$, *Quat. Sci. Rev.*, 23(14–15), 1513–1522, doi:10.1016/j.quascirev.2004.03.006.
- Stocker, T. F. (1998), Climate change: The seesaw effect, *Science*, 282(5386), 61–62, doi:10.1126/science.282.5386.61.
- Stocker, T. F., and S. J. Johnsen (2003), A minimum thermodynamic model for the bipolar seesaw, *Paleoceanography*, 18(4), 1087, doi:10.1029/2003PA000920.
- Stocker, T. F., et al. (2007), Effects of salt compensation on the climate model response in simulations of large changes of the Atlantic meridional overturning circulation, *J. Clim.*, 20(24), 5912–5928, doi:10.1175/2007JCLI1662.1.
- Stouffer, R. J., et al. (2006), Investigating the causes of the response of the thermohaline circulation to past and future climate changes, *J. Clim.*, 19(8), 1365–1387, doi:10.1175/JCLI3689.1.
- Stuut, J.-B., et al. (2005), Provenance of present-day eolian dust collected off NW Africa, *J. Geophys. Res.*, 110, D04202, doi:10.1029/2004JD005161.
- Timmermann, A., et al. (2007), The influence of a weakening of the Atlantic meridional overturning circulation on ENSO, *J. Clim.*, 20(19), 4899–4919, doi:10.1175/JCLI4283.1.
- Zarriess, M., and A. Mackensen (2010), The tropical rainbelt and productivity changes off northwest Africa: A 31,000-year high-resolution record, *Mar. Micropaleontol.*, 76(3–4), 76–91, doi:10.1016/j.marmicro.2010.06.001.
- Zhang, R. (2007), Anticorrelated multidecadal variations between surface and subsurface tropical North Atlantic, *Geophys. Res. Lett.*, 34, L12713, doi:10.1029/2007GL030225.

J. Groeneveld, A. Mackensen, and M. Zarriess, Alfred Wegener Institute for Polar and Marine Research, Am Alten Hafen 26, D-27568 Bremerhaven, Germany. (michelle.zarriess@awi.de)

H. Johnstone, S. Mulitza, M. Prange, and S. Steph, Center for Marine Environmental Sciences, University of Bremen, Leobener Straße, D-28359 Bremen, Germany.